Journal of Alloys and Compounds 858 (2021) 158314

Contents lists available at ScienceDirect

Journal of Alloys and Compounds

journal homepage: www.elsevier.com/locate/jalcom

Atomic layer deposited Mo_2N thin films using $Mo(CO)_6$ and NH_3 plasma as a Cu diffusion barrier

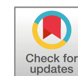

Yong-Hwan Joo[a,1], Dip K. Nandi[a,1], Rahul Ramesh[a], Yujin Jang[b], Jong-Seong Bae[b], Taehoon Cheon[a,c], Soo-Hyun Kim[a,*]

[a] School of Materials Science and Engineering, Yeungnam University, 214-1, Dae-dong, Gyeongsan 712-749, South Korea
[b] Busan Center, Korea Basic Science Institute, 1275 Jisadong, Gangseogu, Busan 618-230, South Korea
[c] Center for Core Research Facilities, Daegu Gyeongbuk Institute of Science & Technology, Sang-ri, Hyeonpung-myeon, Dalseong-gun, Daegu 711-873, South Korea

ARTICLE INFO

Article history:
Received 27 August 2020
Received in revised form 9 December 2020
Accepted 11 December 2020
Available online 15 December 2020

Keywords:
Mo_2N thin films
$Mo(CO)_6$
Plasma power
Resistivity
Diffusion barrier

ABSTRACT

Thin films of molybdenum nitride (Mo_2N) are prepared using sequential exposure of molybdenum hexacarbonyl [$Mo(CO)_6$] and NH_3 plasma in a plasma-enhanced atomic layer deposition (PEALD) reactor. Several process parameters such as the deposition temperature, plasma power, and post-annealing conditions are systematically investigated to achieve the best quality films. The superior growth kinetics is evident with a significantly higher growth per cycle (GPC) value with lower incubation period for this PEALD process (~1.1 Å, ~36 cycles) when compared to thermal ALD (~0.3 Å, ~63 cycles), both carried out at 200 °C. The growth rate of the Mo_2N film reveals a significant jump above 215 °C, indicating a severe decomposition of $Mo(CO)_6$, however, polycrystalline γ-Mo_2N films with face-centered-cubic structure are evident within the deposition temperature range of 200–230 °C. The sharp decrease in the resistivity of the as-grown Mo_2N films is observed with increasing deposition temperature, film thickness, and plasma power. The resistivity could be further lowered by a post-annealing process and the lowest resistivity of ~395 μΩ cm is achieved for the thin film deposited with 300 watt plasma power and annealed at 700 °C. Finally, the Cu-diffusion barrier capability of an extremely thin film (~7 nm) of as-deposited Mo_2N is evaluated in Cu/PEALD-Mo_2N/Si structure. The X-ray diffractometry analysis confirms that such a thin layer can successfully prevent the diffusion of Cu up to 500 °C and significant Cu_3Si formation was observed only at 600 °C and above. The gradual failure of the diffusion barrier upon annealing is further investigated using electrical impedance (EI) analyses in two different modes. In-plane EI measurements directly indicate the change in the Cu layer at the top, and the formation of Cu_3Si can be inferred from the through-plane mode. A comparison with PEALD and thermal-ALD-grown MoN_x from EI analyses further reflects the superiority of plasma-enhanced process towards fabricating diffusion barrier layer.

© 2020 Elsevier B.V. All rights reserved.

1. Introduction

Transition metal nitrides (TMNs) and their thin films have been extensively applied in the field of microelectronics and in several industrial tools for a long time owing to their exciting physical and mechanical properties [1–3]. In relatively more recent times, TMNs have also played a significant role in the field of energy harvesting/storage devices owing to their several excellent properties [4–6]. In general, TMNs are of particular interest because of their low resistivity and high catalytic properties [7,8]. Among several other TMNs (e.g. TiN, TaN_x, WN_x, etc.), molybdenum nitride (MoN_x) also finds potential applications as a hard superconducting material, and in the field of renewable energy which includes secondary batteries, supercapacitors, and as catalysts for H_2 production through water-splitting [9–13]. Several stable phases exist for molybdenum nitride that includes body-centered cubic (bcc) β-Mo_2N, face-centered cubic (fcc) γ-Mo_2N and hexagonal δ-MoN among which γ-Mo_2N could be found to be the most common crystalline phase.

MoN_x thin films were also successfully investigated as copper (Cu) diffusion barriers [14,15]. Cu is commercially used as an interconnect material in the current semiconductor devices due to its several excellent properties like low resistivity and high electromigration resistance. However, owing to its easy reaction with

* Corresponding author.
E-mail address: soohyun@ynu.ac.kr (S.-H. Kim).
[1] These authors contributed equally.

https://doi.org/10.1016/j.jallcom.2020.158314
0925-8388/© 2020 Elsevier B.V. All rights reserved.

silicon (Si) to form copper silicide at a relatively low temperature and hence requires a thin diffusion barrier layer of suitable material like MoN_x. On the other hand, as the size of the integrated circuits continuously gets reduced, the barrier layer thickness must also reduce in proportion and the dimension of it goes well below 10 nm [16,17]. Therefore, preparing high-quality, stoichiometric crystalline MoN_x thin films with precise thickness control at low deposition temperature is of importance. As we already mentioned, a process that delivers high-quality MoN_x thin film could also be very useful for several energy-related applications. The MoN_x thin film was mainly deposited by sputtering and chemical vapor deposition (CVD) [18–24]. In the case of sputtering, typically, N_2 and Ar gas mixture with various gas flow rates and metallic Mo target are employed. While sputtering enabled the deposition at low/room temperature, the deposited films sometimes suffered from high resistivity (500–1,250 μΩ cm) and amorphous phase [18,20]. However, sputtering also provides a easy room to deposit these films with different amounts of N-content (or different crystalline phases) and even as a mix-phase of Mo and MoN_x [21–23]. On the other hand, CVD of molybdenum nitride takes place at a relatively higher temperature ranging from 300° to 850 °C. It typically uses MoF_6, $MoCl_5$ and $Mo(CO)_6$ as precursors for the MoN_x thin film deposition [24,25]. But, in principle, it is considered that the line-of-sight physical vapor deposition (PVD) process like sputtering has an inherent disadvantage of poor step coverage and eventually fails to apply at higher aspect ratios. Moreover, the exact control of thickness and uniformity of the film are becoming more difficult issues as the barrier thickness is reduced below ~10 nm. Although the CVD process can be applied to give improved step coverage, it also suffers from other disadvantages such as the incorporation of unintentional corrosive impurities in the film like Cl and F and relatively high deposition temperature.

Apart from the above-mentioned methods, MoN_x is also successfully deposited with atomic layer deposition (ALD), a technique capable of controlling the film thickness up to sub-nm level with high uniformity and with excellent step coverage [26–28]. A self-limiting surface reaction chemistry of ALD process where the reactants are dosed separately into the chamber to grow a desired film, attracts significant amount of research in recent times in the field of energy as well as in semiconductor industries [29,30]. Despite a strong need, only a few studies have been reported to develop ALD-MoN_x processes. MoN_x films were earlier deposited with $MoCl_5$ and 1,1-dimethyl-hydrazine (DMHy) or NH_3 at a deposition temperature ranging from 350° to 500 °C [26,31]. It was shown that $MoCl_5$ not only provided low resistivity (below 500 μΩ cm) MoN_x films with reasonably low Cl content, but also could be used as a Cu-diffusion barrier up to ~600 °C. Later, ALD of MoN_x thin films were carried out using metal-organic precursors, $Mo(N^tu)_2(S^tBu)_2$ and $Mo(CO)_6$ which enabled to avoid any corrosive by-products during the reaction [27,28]. In addition, these precursors enabled the film deposition at relatively lower deposition temperature below 300 °C but also resulted in amorphous films. Our recent studies further revealed that $Mo(CO)_6$ could be successfully used to prepare MoN_x films for several different applications [32–35]. However, these thermal ALD grown MoN_x films generally contains significant amount of oxygen in the film and hence the resistivity of these films were found to be extremely high [35].

In this study, we evaluated the ALD of MoN_x using NH_3 plasma as a reactant for the first time with molybdenum hexacarbonyl [$Mo(CO)_6$] as a Mo-precursor. To the best of our knowledge, there is no report till date on PEALD of MoN_x. Several process parameters like deposition temperatures, different plasma powers, and post-annealing of the as-grown films were carried out to find the optimal ALD process to achieve the best quality thin film. Finally, the thin film of MoN_x was deposited in Cu/PEALD-MoN_x/Si structure to verify its diffusion barrier performance against copper and compared with thermal-ALD grown MoN_x films with the help of electrical impedance studies.

2. Experimental

2.1. Deposition

MoN_x thin films were deposited in a shower-head type ALD reactor (Lucida-M100, NCD Technology) on Si substrate with ~100 nm thermally grown SiO_2 layer. In general, one ALD cycle consists of four individual steps, namely the precursor injection pulse, precursor purge, reactant injection pulse, and reactant purge. While molybdenum hexacarbonyl [$Mo(CO)_6$] is used as a metal precursor here, the reactant is ammonia (NH_3) plasma. $Mo(CO)_6$ is a white powder at room temperature with negligible vapor pressure and therefore, to increase its vapor pressure, the bubbler containing this precursor was kept at 40 °C. In addition, an overhead Ar gas (50 sccm) was used as a carrier gas to carry $Mo(CO)_6$ smoothly into the chamber. NH_3 plasma (50 sccm) was generated by applying a radio frequency (RF) powers of 100–300 watt (W) to the shower-head at the reactant pulsing step to complete the reaction. The ALD chamber temperature was varied from 180° to 230 °C, and the working pressure was maintained at 0.4 Torr. The basic ALD condition of this study was set as follows; Mo precursor pulsing of 10 s, precursor purging of 10 s, NH_3 plasma reactant pulsing of 10 s, and reactant purging of 10 s

2.2. Analysis of films properties

Various analytical methods were used to confirm the growth characteristics and physical properties of MoN_x thin films. The thickness of the grown film was measured by cross-sectional field emission scanning electron microscopy (FE-SEM, Hitachi S-4800 with the voltage at 10 kV). Phase and crystallinity of the MoN_x thin films were established by X-ray diffraction (XRD, PANalytical X′pert PRO MRD with Cu Kα radiation at 1.5 kW). The sheet resistances of the films were measured using a four-point probe. X-ray photoelectron spectroscopy (XPS, ESCALAB 250 spectrometer at the Korea Basic Science Institute Busan) using an Al K_α source was used to confirm the surface composition, impurity, and the oxidation state of molybdenum and nitrogen. The diffusion barrier test sample was prepared by removing the native oxide (SiO_2) on Si wafer by 10 min HF treatment and then growing a MoN_x thin film followed by depositing ~7 nm Cu layer on top of it. Plan-view and cross-sectional view transmission electron microscopy (TEM, Hitachi HF-3300) analysis for the as-grown Mo_2N films and Cu/MoN_x/Si structure was performed to confirm the microstructure and the desired thickness of the ultrathin barrier layer, respectively. To improve the physical properties and crystallinity of the MoN_x thin film, annealing was carried out in a rapid thermal annealing furnace (RTA, Infovision, halogen lamp as the heating source) system under H_2 (20 sccm) atmosphere at 500–700 °C for 10 min. The diffusion of Cu at various temperature was monitored by analyzing the formation of copper silicide using XRD, and electrical impedance measurements. Impedance measurements were recorded in both in-plane and through-plane modes, the spectra were recorded with an alternating current root-mean-square (rms) amplitude of 5 mV in the frequency range of 0.1–50 mHz and with a data collection interval of 10 points per decade.

3. Results and discussion

3.1. Growth of MoN_x using $Mo(CO)_6$ and NH_3 plasma

The thermal stability of the $Mo(CO)_6$ precursor was first evaluated by varying the deposition temperature in the range of 180–230 °C (Fig. 1a). Under the basic pulsing condition (precursor pulsing of 10 s, reactant pulsing of 8 s, precursor and reactant purging of 10 s), by measuring the thickness of MoN_x films, the growth per cycle (GPC) is estimated. When the deposition temperature was

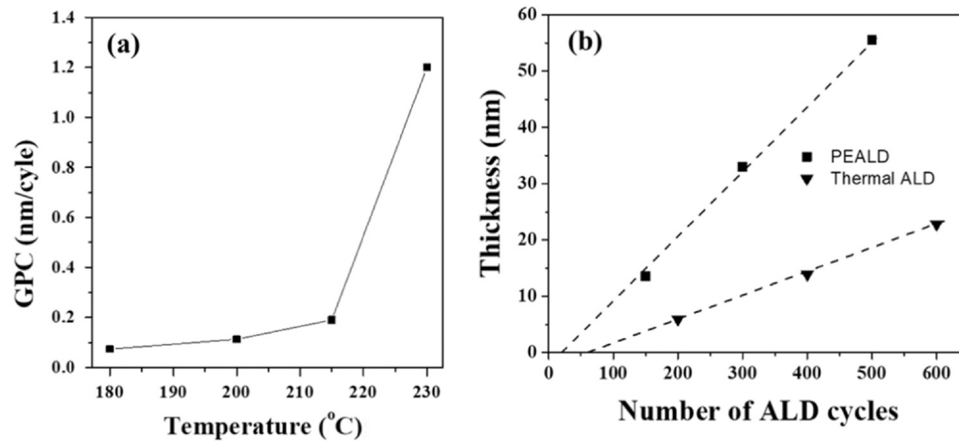

Fig. 1. (a) GPC as a function of ALD chamber temperature and (b) the thickness of PE- and thermal-ALD MoN_x films grown at 200 °C as a function of the number of ALD cycles showing significantly higher GPC with lower incubation period for PEALD process. Thermal ALD data is taken from reference [34] for comparison.

180 °C, the GPC was found as ~0.074 nm. Increasing the deposition temperature to 200 °C, the GPC increased to a value of ~0.11 nm. Similarly, the GPC did not increase drastically when the deposition temperature becomes 215 °C. However, a further increase in the deposition temperature to 230 °C results in a quantum jump in the GPC (~1.21 nm), indicating that the severe/complete decomposition of $Mo(CO)_6$ at this temperature under this reaction condition. The earlier report from our group on thermal ALD of MoN_x using this precursor discussed in detail about the decomposition related issues associated with $Mo(CO)_6$ [35]. However, a significant change in the growth kinetics when NH_3 plasma is used in place of its gas can be easily comprehended. Here, one should also notice that the variation in the GPC values of the films grown within a deposition temperature of 180–215 °C might be considered as ALD-like deposition when compared to the extremely high GPC (~1.2 nm) beyond 215 °C. Therefore, though there might be a fraction of CVD type growth in this process even at the lower limit of the deposition temperature, we consider a predominant PEALD process at least up to 215 °C. It is also noteworthy to mention here that the $Mo(CO)_6$ precursor and NH_3 molecules (thermal ALD) delivered a much lower GPC of ~0.03 nm at 200 °C. Next, the linearity of thin-film growth is demonstrated by depositing MoN_x at 200 °C with an increasing number of ALD cycles (Fig. 1b). For comparison, the figure also includes the growth linearity during thermal-ALD of MoN_x at the same deposition temperature. Both of the curves show a linear dependence of the film thickness with the number of ALD cycles with a significant difference in GPC and the incubation period. While the incubation cycles number was found to be ~36 during PEALD, it was estimated around 63 cycles for thermal-ALD. Hence, the incubation period identified with the PEALD process was significantly lower than that of our earlier reported process of thermal ALD-MoN_x [35]. Therefore, the presence of plasma not only enhances GPC significantly but also influences the overall reaction kinetics (including the initial nucleation process) when compared to its thermal ALD counterpart. Next, we have studied in detail the film's properties (crystallinity and resistivity) depending on a few process parameters and after post-annealing. The deposition temperature was primarily chosen as 200 °C for detailed studies at the rest of the work including the Cu-diffusion barrier application. However, the preliminary properties (resistivity and crystallinity) were also evaluated of the as-deposited films grown above 200 °C.

3.2. Properties of PEALD-MoN_x and post-annealing

The electrical resistance of the deposited thin film is one of the important criteria for the application in the diffusion barrier to Cu. Therefore, the resistivity of the as-grown MoN_x films was studied in detail. The resistivity of these PEALD grown thin films was determined by multiplying the sheet resistance measured on a 4-point probe by the thickness of the film determined from the SEM analysis. Fig. S1 shows a couple of cross-sectional view SEM images of the as-grown MoN_x films on Si/SiO_2 substrates deposited at two different temperatures with two different cycles. Uniform, continuous, pinhole free dense films are evident from these images. Fig. 2a shows

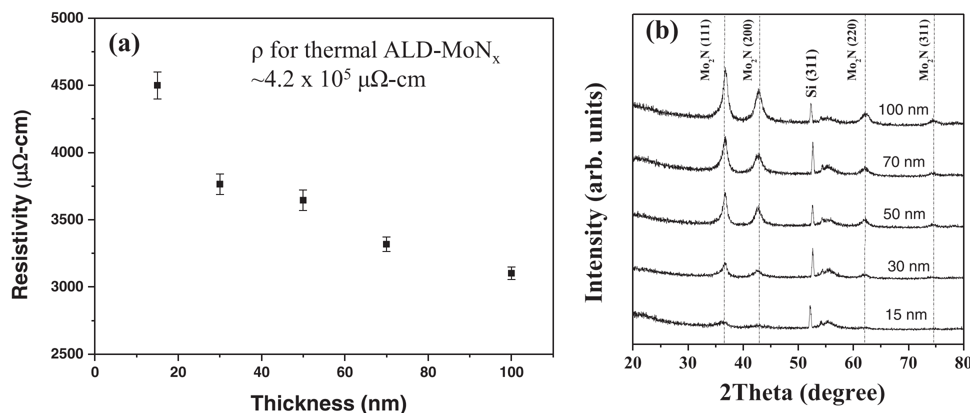

Fig. 2. (a) The resistivity and (b) corresponding X-ray diffraction (XRD) patterns of PEALD-MoN_x thin films grown at 200 °C with the thickness which can be controlled by the number of ALD cycles.

the resistivity on as-grown MoN_x thin films as a function of the film thickness (deposited at 200 °C). The resistivity significantly decreased from ~4,500 μΩ cm to ~3,100 μΩ cm with increasing the thickness from ~15–100 nm by varying the ALD cycles from 150 to 1,000 cycles. The reduction in the resistivity is more at the beginning and the variation is expected to slow down reasonably beyond film thickness of ~100 nm. The resistivity of these as-grown films at 200 °C is still high above the bulk/lowest resistivity of pure Mo_2N films reported earlier. Nevertheless, the resistivity was also observed to decrease rapidly with increasing deposition temperature (Fig. S2). The sharp reduction in the resistivity could lead to a value as low as ~665 μΩ cm for the film grown at 230 °C. A similar observation was earlier reported during ALD of MoN_x using $MoCl_5$ and $Mo(CO)_6$ [31,35]. However, keeping in mind the severe decomposition of the precursor at this temperature, one may think of some potential applications where extremely controlled, smooth, conformal film is not required. If a bulk (thick) film with somewhat rough surface does not limit one's applications, a CVD-like growth with this recipe would be better. A similar decreasing trend with an increasing thickness (ALD cycles) was observed with resistivity values for the films grown at 230 °C as shown in Fig. S3 and a lowest resistivity of less than 400 μΩ cm could be achieved for a film with a thickness above 150 nm. Fig. S4 shows a cross-sectional view SEM image of a thick MoN_x film (~140 nm) grown at 230 °C revealing a relatively rough surface but the dense film is evident. We have also measured these sheet-resistances over time and observed a nominal increase in the values after 24 hr as shown in Table S1. Thereafter, the further changes are truly negligible indicating that the films are quite stable in the atmosphere with a minimum surface contamination (or oxidation) at the beginning. Finally, it is noteworthy to mention here that the measured resistivity values are far lower when compared to MoN_x thin films deposited with thermal ALD, which was ~420 m Ω cm for the film deposited at 200 °C. This clearly suggests that MoN_x thin film deposited with PEALD are of much superior electrical properties than that of thermal ALD using $Mo(CO)_6$ precursor. Thermal ALD-grown MoN_x (at 225 °C and above) could provide a similar order of resistivity (~3,900 μΩ cm) only after post-annealing at a high temperature of 700 °C in NH_3 environment.

The XRD patterns of as-grown PEALD-MoN_x on the Si/SiO_2 substrate were obtained in a GIAXRD configuration in the 2θ range of 20–80°, the results are displayed in Fig. 2b. As the thickness of the thin film increases from 15 nm to 100 nm, the XRD peak intensity increases linearly. The XRD results showed three distinct peaks centered at around 37°, 43°, 63° which could be matched to (111), (200), and (311) planes, respectively, of γ-Mo_2N. This indicates that the as-grown films using PEALD gives rise to well-defined polycrystalline phase of molybdenum nitride and it further confirms the higher quality film formation when NH_3 plasma is used as a reactant in place of NH_3 molecules (or thermal ALD). A similar observation has been seen for thermal-ALD/PEALD of MoS_2 using $Mo(CO)_6$. Therefore, unlike to thermal ALD, the presence of plasma not only brought down the deposition temperature but also helped to form crystalline film even at 200 °C. The XRD profiles at different depositions temperatures are also shown in Fig. S5 which reveals an increase in the crystallinity of the films with increasing deposition temperatures. The variations in the properties (both resistivity and crystallinity) might appear due to the different thicknesses of the films (all the films are grown with same ALD cycles which leads to thicker films at higher deposition temperature). However, the lower resistivity films at higher deposition temperatures should also come from a better quality of the films at that temperature and such observation are not uncommon. Further, the plan view TEM analyses are carried out to unveil the microstructure of the films as shown in Fig. 3 for the as-grown films deposited with 100 W power. The bright-field (BF) TEM images at different magnifications (Fig. 3a–c) show a uniform distribution of the crystal grains in the film with an average size of ~15–30 nm. Though a similar kind of microstructure was observed earlier for PEALD grown Mo_2N using Mo $(N^tBu)_2(S^tBu)_2$, the average grain size estimated in the current study is considerably higher [15]. In addition to these BF-TEM images, one dark-field TEM image is shown in the inset of Fig. 3a depicting further the crystalline nature of the film. Moreover, the selected area electron diffraction (SAED) pattern of the film is included in the inset of the Fig. 3c. It reveals the polycrystalline nature of the film, which generates co-centric bright diffraction rings, ascribed to the three major planes, (111), (200), and (220) of γ-Mo_2N.Finally, the high-resolution TEM (HR-TEM) image clearly exhibits the crystal lattice and the corresponding planes could be determined from the *d*-spacing calculation as shown in Fig. 3d.

The PEALD-Mo_2N process was further performed as a function of plasma power at a fixed deposition temperature (200 °C). Fig. 4a shows that as the plasma power increases from 100 to 300 W, the resistivity of the deposited film decreases from ~4,200–1,900 μΩ cm. The use of NH_3 plasma generates highly reactive radical species such as NH_x^*, H^*, N_2^*, H_2^* and electrons, which will improve the overall reaction kinetics during the film's growth [36,37]. The intensities of various species and electrons increases with increasing plasma power which is believed to improve the overall films properties. Fig. 4b shows the results of XRD analysis of the MoN_x thin films deposited at plasma powers of 100, 200, and 300 W. It is evident that at the higher plasma powers (200 and 300 W), the as-grown films form similar Mo_2N structure which was also observed earlier with 100 W. However, it could be now seen that there is a considerable increase in the XRD peaks reflecting an improvement in the crystallinity of the grown thin film with increasing plasma power from 100 to 300 W. The decrease in film's resistivity with increasing plasma power was also observed during reactive dc magnetron sputtering of the Mo_2N thin films [19]. The increase in the reactive species with increasing plasma power will aid in the formation of highly dense film and consequently results in the improvement in the thin film resistivity with the increase in the plasma power. The BF-TEM images obtained for the films deposited with different plasma powers (Fig. S6a, c, e) reveals the formation of more densely packed grains with increasing plasma power while the similar polycrystalline nature of the films remain intact (Fig. S6b, d, f). Therefore, higher plasma power is more effective to deposit Mo_2N thin films in PEALD and the current experimental set-up highest plasma power of 300 W provides a denser film with better crystallinity and lower resistivity.

Next, we want to explore the effect of N_2/H_2 mixture plasma (at highest plasma power possible, 300 W) on the as-grown film's resistivity. As higher plasma power is expected to grow the films at a relatively lower temperature, the variation of co-reactants was investigated at a deposition temperature of 180 °C with 500 ALD cycles. Fig. 5 shows the resistivity of the as-grown films deposited with different plasma. The highest resistivity of ~5,000 μΩ cm the film was obtained with NH_3 plasma and once it is replaced with N_2/H_2 mixture plasma the resistivity decreases significantly as can be seen from Fig. 5. Three different ratios with increasing H_2 percentage were further carried out and it was observed that the film resistivity was continuously decreased with decreasing N_2 to H_2 ratio. While ca. 1,964 μΩ cm resistivity was obtained with (1:3) N_2/H_2, the lowest resistivity of ~627 μΩ cm was achieved with (1:10) N_2/H_2 mixture plasma. However, lowering the resistivity using mixture plasma might also lead to change the overall composition/phase of the film making a combination of MoC_xN_y or even Mo_2C. A mixture plasma of N_2/H_2 is known to give such films during ALD performed with metal-organic precursor [38]. To know the detailed composition, XPS was performed for the films grown with NH_3 plasma and with two different ratios (1:3 and 1:10) of N_2/H_2 mixture. The complete survey spectra before and after Ar sputtering (for 60 s) of the as-grown films deposited with NH_3 plasma is shown in Fig. S7. Along with Mo and N

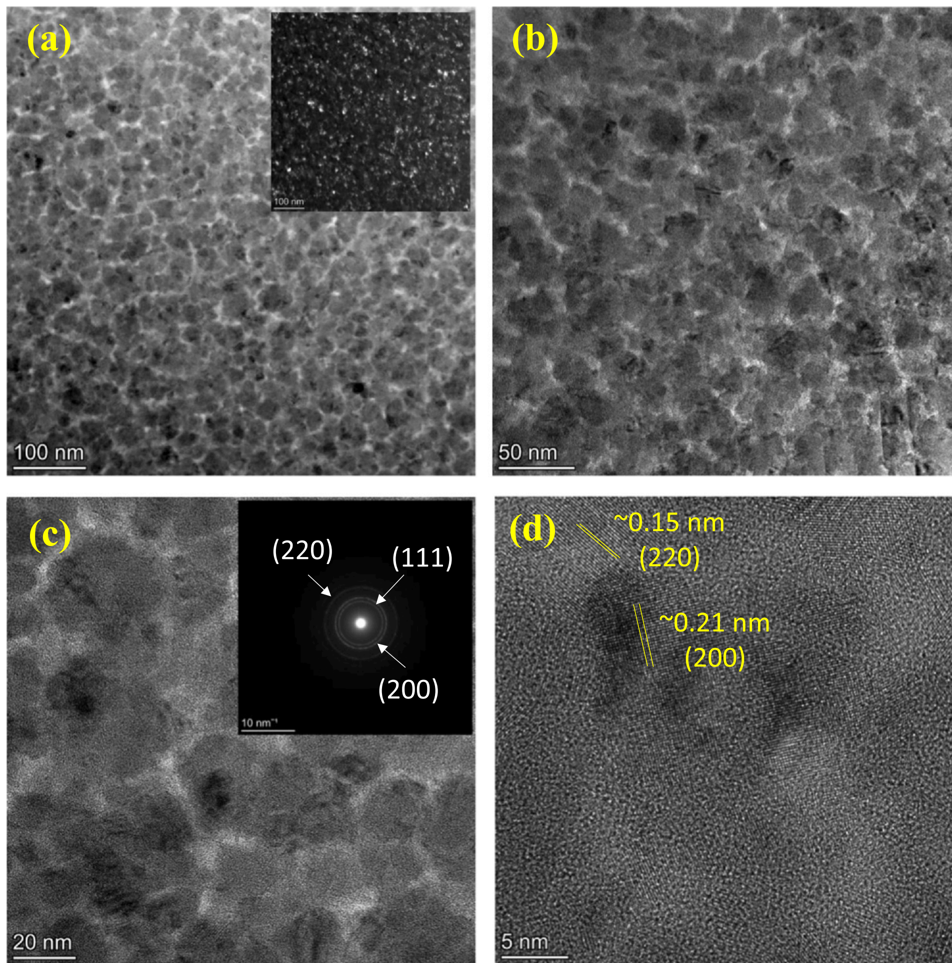

Fig. 3. (a–c) Bright-field TEM images with three different magnifications of the Mo_2N film deposited with 100 W plasma power and in inset of (a) the dark-field image, (c) the SAED pattern, (d) HRTEM image of the same film showing the different crystal planes of Mo_2N.

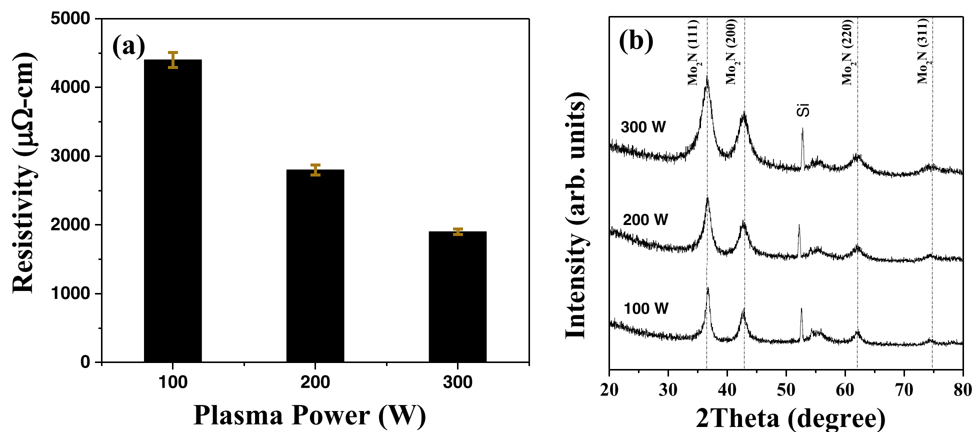

Fig. 4. (a) The resistivity and (b) X-ray diffraction (XRD) patterns of PEALD-MoN_x thin films (grown at 200 °C) as a function of plasma power.

peaks, O 1*s* and C 1*s* peaks were clearly identified in the spectra for the film without sputtering. It is very much expected that these elements would be present as a surface contamination at the top of the film and hence an Ar sputtering of a few nm of the film is recommended. While the peak corresponds to C was almost disappeared after etching the film's surface with Ar sputtering, a less intense peak for O 1*s* remains after sputtering. The presence of O in the near-surface or bulk of the film might come from the CO ligands of the Mo-precursor or the oxygen diffusion while the film was exposed to the environment. However, as there was not considerable C in the bulk of the film, the most probable source of this O is external and not from the precursor. Fig. 6 further shows the high-resolution XP-spectra of Mo 3*d*, Mo 3*p*-N1*s*, and C 1*s* of three different samples. The spectra were recorded after Ar-sputtering to avoid surface contamination and to have more precise information about the actual composition of the respective film. For the sample deposited with NH_3 plasma, two strong peaks appear at approximately 228.9 eV and 231.9 eV due to the Mo *3d* orbital electrons

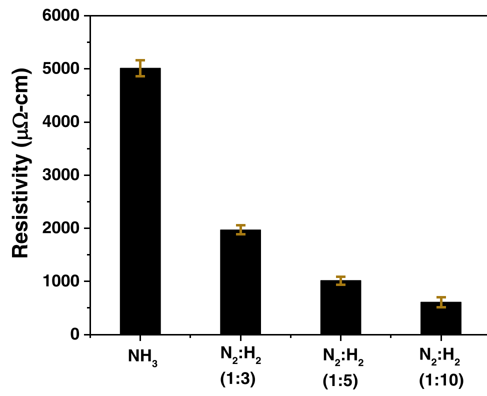

Fig. 5. The resistivity of the as-grown films with NH_3 plasma and N_2 and H_2 mixture plasma with different ratio, deposition temperature (180 °C) and plasma power (300 W) kept fixed for all the reactions.

(Fig. 6a) in the Mo–N bond of Mo_2N corresponding to Mo $3d_{5/2}$ and Mo $3d_{3/2}$, respectively. There was not any noticeable shift of these peaks for the sample deposited with (1:3) N_2/H_2 mixture plasma. However, both of these Mo3d peaks shifted to lower binding energies indicating molybdenum carbide formation when the film was grown with (1:10) N_2/H_2 mixture plasma. The center of the peaks for Mo 3*d* orbital electrons located at BEs of 228.4 and 231.4 eV corresponding to $3d_{5/2}$ and $3d_{3/2}$, respectively could be considered to the XPS peaks coming from Mo-C [39]. Therefore, the XPS analysis of Mo3d peaks indicates the formation MoC_xN_y with N_2/H_2 mixture-plasma as a co-reactant.

More convincing information could be further drawn from Mo3*p*-N1*s* high-resolution XPS. Two distinct peaks shown in Fig. 6b at 394.8 eV and 397.1 eV can be assigned to of Mo $3p_{3/2}$ and N *1s*, respectively, of the Mo–N bonding for the sample deposited only with NH_3 plasma. Now, when N_2/H_2 mixture plasma was used, while the BE position of the N1s (at ~397.1 eV) peak does not shift but the intensity of this peak is found to reduce continuously. Considerably, less intense peak correspond to this N 1*s* electron was observed for the film grown with (1:10) N_2/H_2 mixture-plasma. The reduction in the intensity of the N 1*s* peak could be clearly comprehended with respect to its corresponding Mo 3*p* peak. On the other hand, a clear and similar shift towards the lower BE position of 394.2 from 394.8 eV for Mo $3p_{3/2}$ with increasing N_2/H_2 mixture plasma further confirming the formation of Mo-C bond in the films. Finally, the XPS of C 1*s* ensures the molybdenum carbonitride formation (Fig. 6c). While a very broad, not well-defined peak was observed for the film deposited with NH_3 plasma corresponding to C 1*s*, it could be assigned to some impurity related C-C bond (graphitic carbon at 284.6 eV) in the film. Once NH_3 is replaced with N_2/H_2 mixture plasma [with (1:3) ratio], a slight increase in the intensity of the C 1*s* peak could be inferred. However, a sharp well-defined peak at relatively lower BE of ~282.8 eV was identified for the film deposited with N_2/H_2 ratio of 1:10 and this peak could be ascribed to Mo-C present in molybdenum carbide [40,41]. The presence of C 1*s* in the

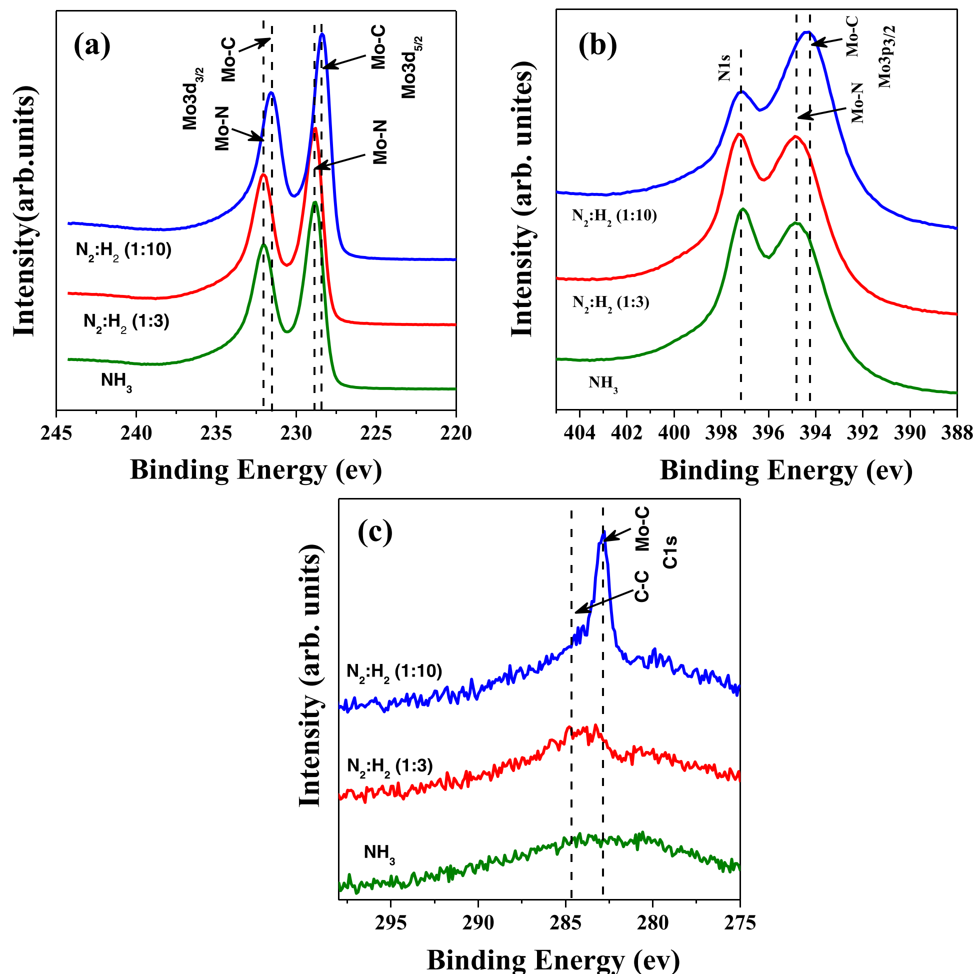

Fig. 6. High-resolution X-ray photoelectron spectroscopy (XPS) of (a) Mo 3d, (b) Mo3p-N1s, and (c) C 1s spectra for the films grown with NH3 plasma, and with two different ratio of N_2/H_2 mixture plasma as a co-reactant.

form Mo-C could be further realized by comparing this peak before and after the Ar-sputtering of the films. While C is more of an impurity on the film's surface deposited with NH_3 plasma, a considerable presence C 1*s* with a shift towards lower BE in the bulk of the film (deposited with N_2/H_2 (1:10) plasma) is evident (Fig. S8). Thus, the XPS analysis reveals that by replacing NH_3 plasma with N_2/H_2 mixture plasma, we can preferably convert the films from pure Mo_2N and to MoC_xN_y and the later would possess lower resistivity than the former. A recent study on CVD of MoC_xN_y using $Mo(CO)_6$ showed an extremely low resistive film preparation for superconducting applications [42]. Therefore, the resistivity of the nitride films would be further reduced by incorporating a controlled amount of C into the film. However, unlike to this study, the carbonitride films were evident only with NH_3. But, PEALD could provide us the opportunity to grow high-quality Mo_2N films as well as MoC_xN_y using different co-reactants. The current work is mainly being focused on molybdenum nitride deposition, and the detailed study of preparing MoC_xN_y can be considered as a future extension of it.

Though the resistivity of the Mo_2N films could be further reduced by varying the co-reactant, but it does not allow us to form pure molybdenum nitride phase. Therefore, to achieve the low resistivity of these pure Mo_2N films, the effect of post-annealing of the as-grown PEALD Mo_2N thin films (deposited with NH_3 plasma) was evaluated. To do so, the films were heat-treated in rapid thermal annealing (RTA) for 10 min in a hydrogen environment. The heat-treatment was performed at 500–700 °C for the Mo_2N thin films grown with 100 and 200 W, whereas, for Mo_2N thin-film deposited with 300 W, the annealing was done up to 900 °C. Fig. 7a shows the resistivity of Mo_2N film as a function of annealing temperature. For all of the samples grown with different plasma powers, the resistivity decreases with increasing annealing temperature and at 700 °C, the resistivity value of all of them is found to be similar (~395 μΩ cm). Such a low resistivity of the Mo_2N thin films will help in applying them in several potential applications either in semiconductor devices or in energy harvesting/storage devices. However, as the highest resistivity of the as-grown film was observed at 100 W plasma power, hence, the rate of change in the resistivity value of this sample with annealing temperature was also highest among three samples. However, 700 °C would be considered as an optimum annealing condition to achieve the Mo_2N films with the lowest resistivity irrespective of their initial growth conditions. On the other hand, it is recommendable to prepare the samples by PEALD with 300 W for this particular process for better quality as-grown films. Keeping this fact in mind, we prefer to anneal the samples grown with 300 W, even at higher temperatures of 800 and 900 °C and measured their resistivity. The results show that the resistivity value does not change considerably at 800 °C but further annealing at 900 °C increases the resistivity of the annealed films. XRD analysis was conducted to determine the cause of the increase in resistivity of this film and Fig. 7b shows the XRD analysis of Mo_2N thin films deposited at 200 °C and 300 W after annealing. While the intensities of the XRD peaks corresponding to Mo_2N increase upon annealing, a new peak also starts appearing at and beyond 600 °C. This peak corresponds to the MoO_2 phase which becomes severe for the sample annealed at 900 °C. The presence of O impurity in the film leads to such oxide phase formation at high temperature which in turn increases the resistivity. From the high-resolution XP-spectra of O 1*s* before and after Ar-sputtering of the as-grown Mo_2N film, one can realize the presence of the O not only in the form of adsorbed OH or CO but in Mo-O (BE centered at ~530 eV) inside the film (Fig. S9). Therefore, annealing beyond 700 °C leads to formation of crystalline-MoO_2 and this temperature should be considered as an optimum temperature for annealing the Mo_2N films to achieve the lowest resistivity.

3.3. Diffusion barrier performances of ALD-MoN_x films against Cu

We have further evaluated the diffusion barrier properties of the as-grown PEALD-Mo_2N thin films (deposited at 200 °C and 100 W) against copper. The experiments were performed on Si substrates after removing the native oxide from the substrate through a 5-minute treatment in HF solution. The barrier layer thickness of Mo_2N was ~7 nm, and Cu (~62 nm thickness) was deposited on top of it through sputtering. Fig. 8a shows the cross-section TEM image of the diffusion barrier test sample. In the TEM image, one can easily see that a very uniform layer (thickness) of Mo_2N thin film is deposited on the Si substrate. Once these samples were successfully prepared, they are annealed at different temperatures ranging from 400° to 700 °C to realize the performance of the barrier layer. Fig. 8b shows XRD patterns of the as-prepared and annealed Cu/PEALD-Mo_2N/Si structures to evaluate the diffusion barrier properties. In the case of as-deposited sample, all of the XRD peaks from Cu film and Si substrate were detected but no peak could be identified corresponding to Mo_2N film owing to its extremely low thickness of ~7 nm. However, the energy dispersive spectra (EDS) confirms the presence of Mo along with other elements (Cu, Si) (Fig. S10) and the N could not be detected probably due to its low atomic weight and hence less sensitivity towards this measurement. When the annealing was performed at 400 °C, no new XRD peaks due to any change in the structure were observed at all, but the intensity of the peaks related

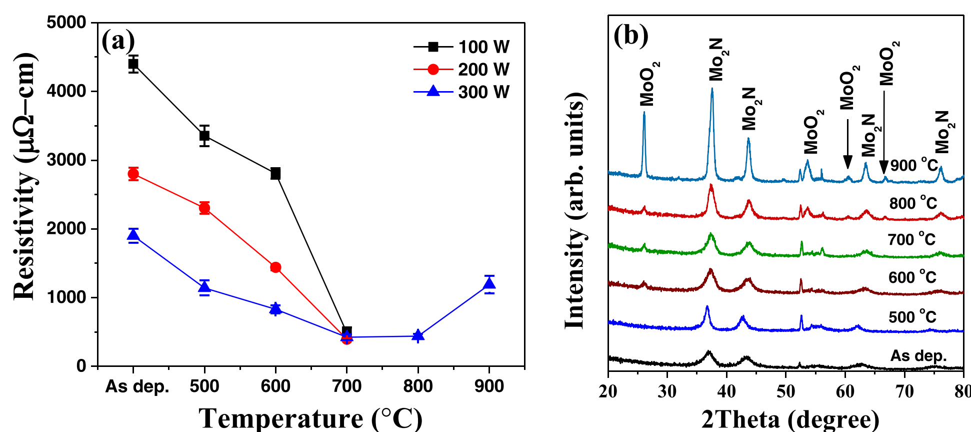

Fig. 7. (a) The resistivity of the PEALD-grown MoN_x thin films as a function of the post-annealing temperature and (b) The corresponding XRD results for the samples deposited with the plasma power of 300 W.

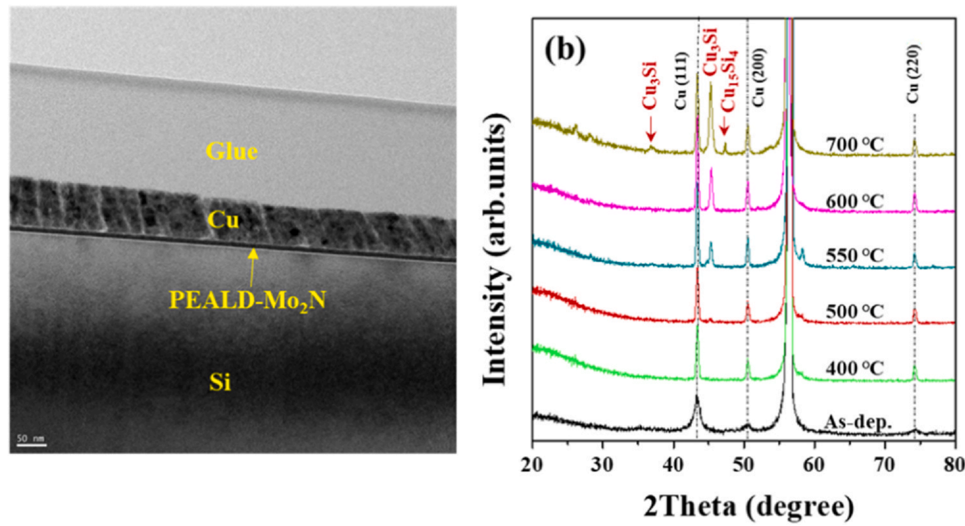

Fig. 8. (a) Cross-sectional view TEM image of Cu/PEALD-Mo_2N/Si test sample before the Cu diffusion barrier test and (b) XRD results of the Cu/PEALD-Mo_2N/Si samples as a function of the annealing temperature.

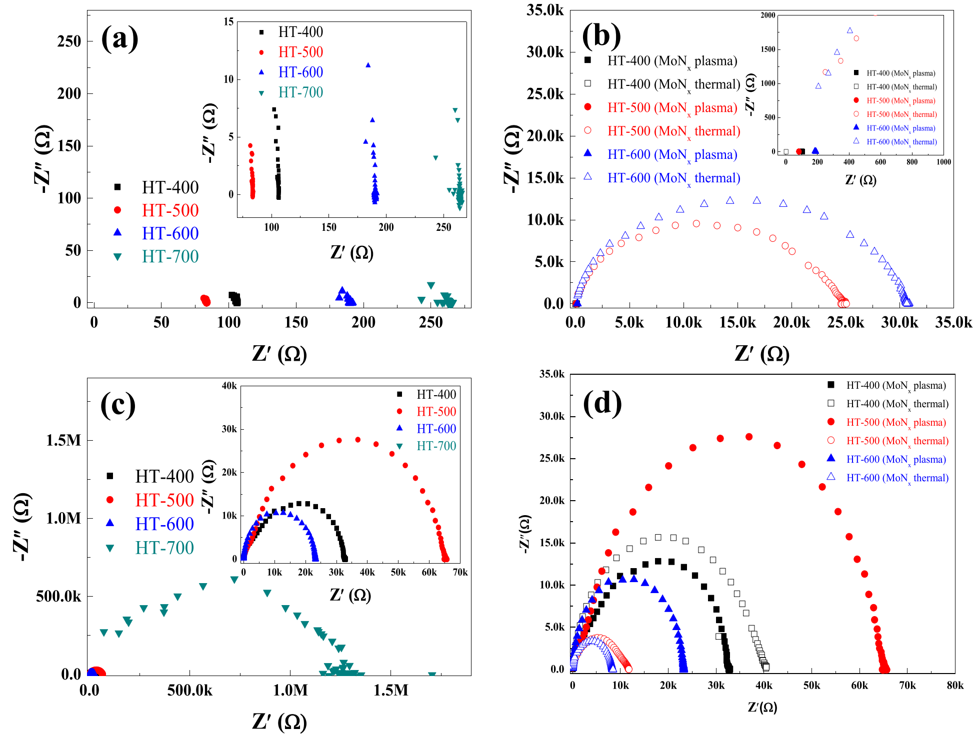

Fig. 9. (a) Electrical impedance analysis (Nyquist plot) of Cu/PEALD-Mo_2N/Si sample in the in-plane mode, (b) comparison of PEALD and thermal ALD MoN_x thin film for Cu diffusion barrier performance by the measurement of in-plane mode, (c) electrical impedance analysis (Nyquist plot) of Cu/PEALD-Mo_2N/Si sample in the through-plane mode, and (d) comparison of PEALD and thermal ALD MoN_x thin film for Cu diffusion barrier performance by the measurement of through-plane mode. Thermal ALD data is taken from reference [34] for comparison.

to Cu increased considerably with a significant reduction in full width at half maximum. This result indicates that the increase in the crystallinity and grain size of Cu due to heat treatment was evident while the Mo_2N layer successfully served as a barrier layer against its diffusion into Si. There were no further changes even after annealing this structure at 500 °C. However, when the 550 °C heat-treated sample was analyzed by XRD, a new peak is formed which can be ascribed as η"-Cu_3Si. This confirms that the failure of the barrier layer has commenced at this temperature. But the low intensity of this copper silicide peak also hints at a very low degree of damage in the structure. Failure of diffusion barrier properties causes some Cu to diffuse through the Mo_2N layer to react with Si to form a Cu_3Si phase. The failure of the barrier layer only becomes severe as the annealing temperature is increased further up to 700 °C leading to form a more intense and new XRD peaks corresponding to Cu_3Si phase. This study, once again, demonstrated that PEALD-Mo_2N had much better diffusion barrier performance when compared to thermal-ALD grown MoN_x films using the same $Mo(CO)_6$ precursor [35]. However, it was confirmed that the diffusion barrier properties were inferior to those of other ALD processes and sputtering [14,15].

3.4. Electrical impedance analysis on the diffusion barrier performance of the Mo_2N thin films against Cu

The Cu diffusion barrier characteristic of Mo_2N thin-film fabricated by PEALD is also evaluated using electrical impedance (EI) analysis. The results obtained are then compared with MoN_x thin film deposited by conventional thermal ALD [35]. The Cu diffusion and the consequent formation of Cu_3Si with temperature results in the failure of the devices, and this can be evaluated using impedance measurements with in-plane and through-plane modes. The electrical contact with the Cu/PEALD-Mo_2N/Si sample is established using the silver paste as shown in Fig. S11. The in-plane mode (Fig. S10a) measures the impedance (resistance) of the Cu thin-film above the ~7 nm thick PEALD-Mo_2N barrier layer on the silicon substrate. With high-temperature-annealing, the Cu will diffuse to the Si substrate due to the failure of the barrier layer. This results in the loss of in-plane electrical contact because of the formation of crack, loss of Cu, and other changes in the phase, and this is generally reflected in the in-plane mode of impedance as the appearance of a semi-circle or very high impedance. However, in the through-plane mode (Fig. S10b), the electrical characteristic is dominated by the dielectric nature of the silicon substrate, and the failure of the Cu diffusion barrier layer can be inferred from the change in the capacitive behavior (imaginary impedance) of the device. Fig. 9a shows the impedance spectra (Nyquist plots) of Cu/PEALD-Mo_2N/Si sample recorded in the in-plane mode of measurement. The spectra are dominated by the resistive characteristic (real impedance) of the Cu metallic film. A frequency-independent impedance (constant impedance values at all measured frequencies) is observed for all the samples, however, with increasing annealing temperature the real impedance (x-axis values) first decreases, and then shows an increasing trend. The 500 °C annealed sample shows the lowest resistance and it might be due to the better metallic characteristic (fewer surface oxides) or favorable phase/crystalline nature (increase in the grain size) of the Cu coating after 500 °C annealing. Such observation in the impedance measurement is in good agreement with the XRD analysis which shows an enhanced crystallinity of the sputtered Cu layer at the beginning. On the other hand, higher values of real impedance for samples annealed beyond 500 °C is due to the loss of Cu by diffusion to Si substrate at a higher temperature, which results in the crack or non-conducting phase formation within the Cu film. It should be noted that the extent of Cu diffusion is negligible even after the high-temperature annealing, and hence the impedance feature is dominated by the conductivity of Cu. Even though the impedance spectra are dominated by the resistive characteristic of metallic copper, a minor stray capacitive behavior is also evident in the spectra (inset to Fig. 9a). This minor capacitive contribution is from the surface oxides/grain boundaries etc. of the Cu film. Fig. 9b shows the comparison of Cu diffusion barrier property of Mo_2N thin-film grown by PEALD and thermal ALD. The Cu film thickness (~63 nm) and Mo_2N barrier layer thickness (~7 nm) are maintained approximately the same for a better comparison of the two. The sample annealed at 400 °C exhibits predominately resistive characteristics in the in-plane mode of impedance measurement for both thermal and the PEALD grown MoN_x barrier layer. However, samples annealed at 500 °C and 600 °C show completely different results with PEALD and thermal ALD grown barrier layer. In the case of the PEALD grown Mo_2N barrier layer, the impedance spectra are dominated by the resistive characteristic of Cu contact (real impedance, which is frequency independent), whereas, the thermal ALD grown MoN_x samples show semi-circles in the Nyquist plots. This is due to the complete failure of the MoN_x barrier layer prepared by thermal ALD, which results in the loss of Cu from the surface of the device, and the formation of a non-conducting path in the in-plane measurement.

The through-plane impedance spectra of Cu/PEALD-Mo_2N/Si samples annealed at different temperatures are shown in Fig. 9c. In contrast to the in-plane measurement, here the Nyquist plot is dominated by the capacitive behavior of the sample, mainly from the silicon. All the samples show semi-circles in the Nyquist plot due to the coupling of the resistive and capacitive path at different applied AC voltage frequency. Annealing at elevated temperature results in a decrease in the size of the semicircle. Similar results are reported for MoN_x film fabricated by thermal ALD [35]. Here, it should be noted that with 500 °C annealed sample an increase in the size of the semicircle is observed which is not well understood. In principle, a decrease in the semicircle size is expected after post-annealing in through-plane mode once the formation of copper silicide takes place. It was the case after annealing the device at 600 °C confirming a failure in the diffusion barrier at this temperature. On the other hand, a drastically bigger semicircle obtained after 700 °C annealing might appear due to the loss in proper contact after a significant amount of Cu diffusion from the top. Fig. 9d shows the comparison of through-plane impedance characteristics towards the Cu diffusion barrier for the MoN_x barrier layer fabricated by the PEALD and thermal ALD process. The sample annealed at 400 °C (sample before the failure of the barrier layer as per the XRD results) shows semicircles with an almost similar diameter in the Nyquist plot. Annealing at elevated temperature results in the reduction in the size of the semi-circle and the extent of decrease is much more severe in the case of the thermal ALD MoN_x barrier layer when compared to the plasma one. The decrease in the size of the semi-circle can be an indication of Cu diffusion into the Si substrate due to the failure of the barrier layer. As a consequence of Cu diffusion into the Si and formation of Cu_3Si, the dielectric behavior (capacitive) of silicon gets reduced and the overall impedance behavior will be now dominated by the more conductive Cu_3Si phase. The present in-plane and through-plane impedance measurement reflects the importance of the microstructure, crystallinity, and phase of Cu diffusion barrier on its performance. The MoN_x film prepared by thermal ALD is mostly amorphous in characteristic, and contain significant oxygen contamination at the surface, whereas, MoN_x thin film prepared by PEALD is highly crystalline (Mo_2N phase), Mo rich, and probably much denser when compared to MoN_x film prepared with thermal ALD. The Mo_2N thin film grown using PEALD is clearly of better quality than that of thermal ALD and this difference is reflected in the Cu diffusion barrier performance of those films.

4. Conclusions

In this study, $Mo(CO)_6$ and NH_3 plasma are used to establish an efficient PEALD process to prepare molybdenum nitride thin films. Crystalline molybdenum nitride (*cubic* γ-Mo_2N) with remarkably high GPC and short incubation period was obtained compared to those obtained by thermal ALD grown amorphous MoN_x films. While the GPC of PEALD-Mo_2N was found ~0.11 nm, a much lower value of ~0.03 nm was observed during thermal ALD grown MoN_x film using the same precursor at 200 °C. Several process parameters (deposition temperature, plasma power, and post-annealing) were investigated to improve the quality of Mo_2N thin films. The resistivity decreased significantly with increasing plasma power and the post-annealing further lowered the resistivity of thin films deposited at various plasma powers. In addition, preliminary experiments also revealed that MoC_xN_y films with significantly low resistivity is possible to deposit with the help of N_2/H_2 mixture plasma as a co-reactant. The lowest resistivity of ~395 μΩ cm is observed for the Mo_2N films annealed at 700 °C and prepared with 300 W plasma power. On the other hand, annealing at a very high temperature (beyond 700 °C) leads to the formation of crystalline MoO_2 along with Mo_2N phase owing to the O impurity present in the as-deposited film, which results in an increase in the resistivity of the

films. Finally, the application of these PEALD grown Mo_2N films as Cu-diffusion barriers is studied in detail and the failure of the barrier layer is investigated with XRD and electrical impedance spectroscopy analysis. While an increase in the real resistance in in-plane EI analysis indicates a failure in the diffusion barrier, a decrease in the size of the semicircle in through-plane mode complements such a claim. The current study shows that the presence of plasma (or PEALD) improves the growth kinetics and the overall film quality significantly when compared to thermal-ALD grown films using the same metal precursor.

CRediT authorship contribution statement

Y.J. carried out ALD experiments, characterizations of the films, and writing manuscript. D.K.N. analyzed the results, wrote and edited the manuscript. R.R. performed impedance experiments, analyzed and wrote the corresponding results. Y.J. and J.-S.B. performed the XPS measurements. T.H. performed the TEM analyses. S.-H.K. conceived of the project and supervised the whole work.

Declaration of competing interest

The authors declare that they have no known competing financial interests or personal relationships that could have appeared to influence the work reported in this paper.

Acknowledgements

This work was financially supported by the MOTIE [Ministry of Trade, Industry & Energy (#10080651)] and KSRC (Korea Semiconductor Research Consortium) support program for the development of the future semiconductor device and the Advanced Technology Center Program (#10077265) funded by the MOTIE (Ministry of Trade, Industry & Energy) of the Republic of Korea. The precursor used in this study was provided by UP Chemical Co. Ltd., Korea.

Appendix A Supporting information

Supplementary data associated with this article can be found in the online version at doi:10.1016/j.jallcom.2020.158314.

References

[1] M. Wittmer, Properties and microelectronic applications of thin films of refractory metal nitrides, J. Vac. Sci. Technol. A 3 (1985) 1797–1803.
[2] A.T. Santhanam, Application of transition metal carbides and nitrides in industrial tools, in: S.T. Oyama (Ed.), The Chemistry of Transition Metal Carbides and Nitrides, Chapman & Hall, 1996, , https://doi.org/10.1007/978-94-009-1565-7_2
[3] R.S. Ningthoujam, N.S. Gajbhiye, Synthesis, electron transport properties of transition metal nitrides and applications, Prog. Mater. Sci. 70 (2015) 50–154.
[4] S. Dong, X. Chen, X. Zhang, G. Cui, Nanostructured transition metal nitrides for energy storage and fuel cells, Coord. Chem. Rev. 257 (2013) 1946–1956.
[5] Y. Zheng, X. Li, C. Pi, H. Song, B. Gao, P.K. Chu, K. Huo, Recent advances of two-dimensional transition metal nitrides for energy storage and conversion applications, FlatChem 19 (2020) 100149.
[6] M.-S. Balogun, Y. Huang, W. Qiu, H. Yang, H. Ji, Y. Tong, Updates on the development of nanostructured transition metal nitrides for electrochemical energy storage and water splitting, Mater. Today 20 (2017) 425–451.
[7] G.M. Matenoglou, L.E. Koutsokeras, P. Patsalas, Plasma energy and work function of conducting transition metal nitrides for electronic applications, Appl. Phys. Lett. 94 (2009) 152108.
[8] X. Peng, C. Pi, X. Zhang, S. Li, K. Huo, P.K. Chu, Recent progress of transition metal nitrides for efficient electrocatalytic water splitting, Sustain. Energy Fuels 3 (2019) 366–381.
[9] S. Wang, D. Antonio, X. Yu, J. Zhang, A.L. Cornelius, D. He, Y. Zhao, The hardest superconducting metal nitride, Sci. Rep. 5 (2015) 13733.
[10] K. Inumaru, K. Baba, S. Yamanaka, Synthesis and characterization of superconducting β-Mo_2N crystalline phase on a Si substrate: an application of pulsed laser deposition to nitride chemistry, Chem. Mater. 17 (2005) 5935–5940.
[11] B. Zhang, G. Cui, K. Zhang, L. Zhang, P. Han, S. Dong, Molybdenum nitride/nitrogen-doped graphene hybrid material for lithium storage in lithium ion batteries, Electrochim. Acta 150 (2014) 15–22.
[12] W.-F. Chen, K. Sasaki, C. Ma, A.I. Frenkel, N. Marinkovic, J.T. Muckerman, Y. Zhu, R.R. Adzic, Hydrogen-evolution catalysts based on non-noble metal nickel–molybdenum nitride nanosheets, Angew. Chem. Int. Ed. 51 (2012) 6131–6135.
[13] Y. Tan, L. Meng, Y. Wang, W. Dong, L. Kong, L. Kang, F. Ran, Negative electrode materials of molybdenum nitride/n-doped carbon nano-fiber via electrospinning method for high-performance supercapacitors, Electrochim. Acta 227 (2018) 41–49.
[14] J.-Y. Lee, J.-W. Park, Diffusion barrier property of molybdenum nitride films for copper metallization, Jpn. J. Appl. Phys. 35 (1996) 4280–4284.
[15] Y. Jang, J.B. Kim, T.E. Hong, S.J. Yeo, S.J. Lee, E.A. Jung, B.K. Park, T.M. Chung, C.G. Kim, D.J. Lee, H.B.R. Lee, S.H. Kim, Highly-conformal nanocrystalline molybdenum nitride thin films by atomic layer deposition as a diffusion barrier against Cu, J. Alloys Compd. 663 (2016) 651–658.
[16] J.B. Kim, D.K. Nandi, T.H. Kim, Y. Jang, J.-S. Bae, T.E. Hong, S.-H. Kim, Atomic layer deposition of WNx thin films using a F-free tungsten metalorganic precursor and NH_3 plasma as a Cu diffusion barrier, Thin Solid Films 685 (2019) 393–401.
[17] P. Majumder, R. Katamreddy, C. Takoudis, Effect of film thickness on the breakdown temperature of atomic layer deposited ultrathin HfO_2 and Al_2O_3 diffusion barriers in copper metallization, J. Cryst. Growth 309 (2007) 12–17.
[18] V.P. Anitha, S. Major, D. Chandrashekharam, M. Bhatnagar, Deposition of molybdenum nitride thin films by r.f. reactive magnetron sputtering, Surf. Coat. Technol. 79 (1996) 50–54.
[19] L. Stöber, J.P. Konrath, S. Krivec, F. Patocka, S. Schwartz, A. Bittner, M. Schneider, Schmid, Impact of sputter deposition parameters on molybdenum nitride thin film properties, J. Micromech. Microeng. 25 (2015) 074001.
[20] Y. Wang, R.Y. Lin, Amorphous molybdenum nitride thin films prepared by reactive sputter deposition, Mater. Sci. Eng. B 112 (2004) 42–49.
[21] L. Stöber, J.P. Konrath, V. Haberl, F. Patocka, M. Schneider, U. Schmid, Nitrogen incorporation in sputter deposited molybdenum nitride thin films, J. Vac. Sci. Technol. A Vac. Surf. Films 34 (2016) 021513.
[22] T. Wang, G. Zhang, S. Ren, B. Jiang, Effect of nitrogen flow rate on structure and properties of MoNx coatings deposited by facing target sputtering, J. Alloys Compd. 701 (2017) 1–8.
[23] M. Kozejova, V. Latyshev, V. Kavecansky, H. You, S. Vorobiov, A. Kovalcikova, V. Komanicky, Evaluation of hydrogen evolution reaction activity of molybdenum nitride thin films on their nitrogen content, Electrochim. Acta 315 (2019) 9–16.
[24] T. Nakajima, T. Shirasaki, Chemical vapor deposition of tungsten carbide, molybdenum carbide nitride, and molybdenum nitride films, J. Electrochem. Soc. 144 (1997) 2096–2100.
[25] S.L. Roberson, D. Finello, R.F. Davis, Phase control of MoN films via chemical vapor deposition, Thin Solid Films 324 (1998) 30–36.
[26] M. Juppo, M. Ritala, M. Leskela, Use of 1,1-dimethylhydrazine in the atomic layer deposition of transition metal nitride thin films, J. Electrochem. Soc. 147 (2000) 3377–3381.
[27] V. Miikkulainen, M. Suvanto, T.A. Pakkanen, Atomic layer deposition of molybdenum nitride from bis(tert-butylimido)- bis(dimethylamido)molybdenum and ammonia onto several types of substrate materials with equal growth per cycle, Chem. Mater. 19 (2007) 263–269.
[28] D.K. Nandi, U.K. Sen, D. Choudhury, S. Mitra, S.K. Sarkar, Atomic layer deposited molybdenum nitride thin film: a promising anode material for Li ion batteries, ACS Appl. Mater. Interfaces 6 (2014) 6606–6615.
[29] M. Leskelä, M. Mattinen, M. Ritala, Review article: atomic layer deposition of optoelectronic materials, J. Vac. Sci. Technol. B 37 (2019) 030801.
[30] P.O. Oviroh, R. Akbarzadeh, D. Pan, R.A.M. Coetzee, Jen,, New development of atomic layer deposition: processes, methods and applications, Sci. Technol. Adv. Mater. 20 (2019) 465–496.
[31] P. Alén, M. Ritala, K. Arstila, J. Keinonen, M. Leskelä, Atomic layer deposition of molybdenum nitride thin films for Cu metallizations, J. Electrochem. Soc. 152 (2005) G361–G366.
[32] D.K. Nandi, S. Sahoo, T.H. Kim, T. Cheon, S. Sinha, R. Rahul, Y. Jang, J.-S. Bae, J. Heo, J.-J. Shim, S.-H. Kim, Low temperature atomic layer deposited molybdenum nitride-Ni-foam composite: an electrode for efficient charge storage, Electrochem. Commun. 93 (2018) 114–118.
[33] R. Ramesh, D.K. Nandi, T.H. Kim, T. Cheon, J. Oh, S.-H. Kim, Atomic-layer-deposited MoN_x thin films on three-dimensional Ni foam as efficient catalysts for the electrochemical hydrogen evolution reaction, ACS Appl. Mater. Interfaces 11 (2019) 17321–17332.
[34] R. Ramesh, S.Y. Sawant, D.K. Nandi, T.H. Kim, D.H. Kim, S.-M. Han, Y. Jang, M.G. Ha, M.H. Cho, T. Yoon, S.-H. Kim, Hydrogen evolution reaction by atomic layer-deposited MoN_x on porous carbon substrates: the effects of porosity and annealing on catalyst activity and stability, ChemSusChem 13 (2020) 4159–4168.
[35] T.H. Kim, D.K. Nandi, R. Ramesh, S.-M. Han, B. Shong, S.-H. Kim, Some insights into atomic layer deposition of MoN_x using $Mo(CO)_6$ and NH_3 and its diffusion barrier application, Chem. Mater. 3 (2019) 8338–8350.
[36] C.W. Lee, Y.T. Kim, Effects of NH_3 pulse plasma on atomic layer deposition of tungsten nitride diffusion barrier, J. Vac. Sci. Technol. B 24 (2006) 1432.
[37] M.F.J. Vos, G. v Straaten, W.M.M.E. Kessels, A.J.M. Mackus, Atomic layer deposition of cobalt using H_2-, N_2-, and NH_3-based plasmas: on the role of the Co-reactant, J. Phys. Chem. C 122 (2018) 22519–22529.
[38] J.B. Kim, B. Jang, H.-J. Lee, W.S. Han, D.-J. Lee, H.-B.-R. Lee, T.E. Hong, S.-H. Kim, A controlled growth of WN_x and WC_x thin films prepared by atomic layer deposition, Mater. Lett. 168 (2016) 218–222.

[39] J. Qiu, Z. Yang, Q. Li, Y. Li, X. Wu, C. Qi, Q. Qiao, Formation of N-doped molybdenum carbide confined in hierarchical and hollow carbon nitride microspheres with enhanced sodium storage properties, J. Mater. Chem. A 4 (2016) 13296–13306.

[40] K. Oshikawa, M. Nagai, S. Omi, Characterization of molybdenum carbides for methane reforming by TPR, XRD, and XPS, J. Phys. Chem. B 105 (2001) 9124–9131.

[41] H.Y. Chen, L. Chen, Y. Lu, Q. Hong, H.C. Chua, S.B. Tang, J. Lin, Synthesis, characterization and application of nano-structured Mo_2C thin films, Catal. Today 96 (2004) 161–164.

[42] E. Mohimi, K. Canova, Z. Zhang, S. Liu, J.L. Mallek, G.S. Girolami, J.R. Abelson, Low temperature chemical vapor deposition of superconducting molybdenum carbonitride thin films, J. Vac. Sci. Technol. A 37 (2019) 021503.